# Experimental Investigation of a Planar Liquid Film Atomization Under High-Speed Gas Stream

Muhammad Osama *

Posted Date: 12 May 2026

doi: 10.20944/preprints202605.0783.v1

Keywords: primary atomization; liquid film breakup; airblast atomization; gas-liquid shear flow

 doi:10.20944/preprints202605.0783.v1



*Article*

# Experimental Investigation of a Planar Liquid Film Atomization Under High-Speed Gas Stream

**Muhammad Osama**

Department of Mechanical Engineering Wayne State University, Detroit, MI 48202, USA; musama375@wayne.edu

**Abstract**

We present a systematic experimental investigation of the primary breakup of a planar liquid film subjected to high-speed co-flowing gas streams. A water film of thickness $D_\ell \approx 150$ $\mu$m is produced from a symmetric airfoil lip and sheared on both sides by compressed air. Interfacial dynamics were recorded with a high-speed camera and analyzed to extract transverse wavelengths, rupture modes, and their dependence on operating conditions. We find that the transverse wavelength $\lambda_{\text{tra}}$ decreases strongly with increasing gas speed and that, for a given dynamic pressure ratio $M = (\rho_g V_g^2)/(\rho_\ell V_\ell^2)$, different absolute combinations of $V_g$ and $V_\ell$ produce markedly different $\lambda_{\text{tra}}$. These observations indicate that gas-shear intensity and the gas flow instability modes (vortex shedding) control the breakup of the liquid film; the liquid inflow plays a secondary role under our conditions. The results provide experimental benchmarks for model validation and suggest routes to tune atomizer performance via gas-side control.

**Keywords:** primary atomization; liquid film breakup; airblast atomization; gas-liquid shear flow

## 1. Introduction

Air-blast atomization of liquid films, when exposed to high-speed co-flowing gas streams, leads to the production of fine droplets. This phenomenon has a wide range of applications across various industries, including agricultural irrigation, spray painting, gas turbines, and spray coating [1,2]. Given the importance of accurately predicting spray characteristics and optimizing industrial devices, considerable research has been devoted to understanding the breakup dynamics and the mechanisms underlying this process [3–7]. It is shown that the liquid film undergoes oscillations in both the streamwise and spanwise directions, forming longitudinal and transverse waves, driven by Kelvin–Helmholtz (KH) and Rayleigh–Taylor (RT) type instabilities, respectively. As these instabilities grow, the gas flow stretches the liquid film, leading to the formation of hollow bags between transverse waves. These bags eventually rupture into multiple holes, which collide with one another, fragmenting the thin film forming the bag structures into fine droplets and ligaments. This atomization process spans multiple timescales and length scales, including the atomizer lip thickness, film thickness, instability wavelengths, boundary layer thickness, and turbulence scale. As a result, gaining a detailed understanding of these mechanisms is complex, yet essential.

In our previous numerical study [8], we investigated the aerodynamically-driven rupture of a liquid film through three-dimensional numerical simulations. A thin liquid film with a thickness of $h_l = 25\mu$m was used to accelerate the fragmentation process. It is worth noting that this thickness is approximately ten times smaller than the values typically used in experimental studies, e.g. [7,9]. A fixed gas Reynolds number, $Re_g = \rho_g U_g h_l/\mu_g = 5000$, was considered, where $\rho_g$ and $\mu_g$ represent the gas density and viscosity, respectively, and $U_g$ is the gas velocity. We demonstrated that the liquid film is entrained by the fast-moving gas streams, causing it to oscillate and stretch in the longitudinal direction. Small transverse deformations at the liquid interface were observed and attributed to the influence of rib-like vortical structures in the gas flow. Due to the small film thickness considered, bag structures do not form between the transverse waves, as seen in experimental observations []. Instead,

 doi:10.20944/preprints202605.0783.v1



the liquid film between the transverse waves fragments through hole nucleation and subsequent collisions.

Recently in a numerical study [10], we use the same liquid film thickness of 25$\mu$m but vary the gas Reynolds numbers ($Re_g = 300, 500, 1000$) to examine the inertial and viscous effects on the gas flow dynamics and liquid film fragmentation. For the gas flow dynamics, distinct three-dimensional vortex shedding modes are observed depending on $Re_g$. These modes significantly influence the liquid film fragmentation process, controlling the transverse wavelength and the localization of hole formation, which ultimately determines the number of ligaments and the droplet size distribution. This study clearly highlights the pivotal role of instability modes in the gas flow, establishing a direct connection between the gas vortical structures and the breakup process of the entrained liquid film. This novel insight opens the door to enhanced predictive models for air-blast atomization of liquid films.

In the present study, we report a controlled experimental characterization of the transverse instability and primary breakup of a planar liquid film exposed to high-speed, symmetric co-flowing gases. Using synchronized high-speed imaging and precisely metered gas and liquid inflows, we measure the transverse wavelength $\lambda_{\text{tra}}$ to quantify the dependence of these features on $V_g$, $V_\ell$, and the dynamic pressure ratio $M$.

### *1.1. Experimental Set-up and Measurement Techniques*

A planar water film of thickness approximately 150 $\mu$m ($D_{liq}$) and width 45 mm was produced by injecting liquid at velocities $V_\ell = 0.32$–$0.77$ m/s through a symmetric airfoil nozzle with the lip thickness ($D_{Lip}$) of 150 $\mu$m. The schematic of the complete planar liquid-film atomization setup is shown in Figure 1 (a), and Figure 1 (b) shows a zoom in on the NACA airfoil to show the water inlet and outlet.

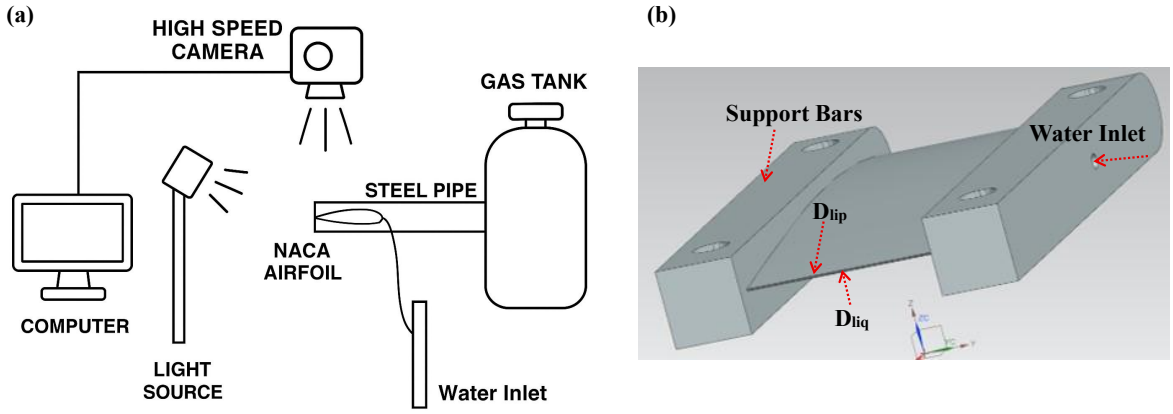


**Figure 1.** (a) Schematic of the planar liquid-film atomization setup. Compressed air enters the steel pipe and is straightened by a honeycomb before shearing the water film on both sides. (b) Zoom in on the NACA airfoil.

Compressed air, regulated via a high-pressure tank and regulator, was delivered to the pipe and accelerated to $V_g = 30$–$64$ m/s on each side of the film. A custom honeycomb insert ($\sim 25$ mm thickness) located 0.5 m downstream of the pipe ensured a uniform, laminar gas profile. Gas velocities were measured with a Fluke 922 Pitot-static tube and flowmeter mounted on a traversing bar, while water flow rates were monitored by a Digiten electromagnetic flowmeter.

Interfacial dynamics were recorded using a Photron Mini UX100 high-speed camera at 10,000 fps (shutter speed 1/100 000 s), with zoom settings of 122.5% and an image resolution of 1280 $\times$ 480 px. Illumination was provided by a 7.2 V, GVM-520S-B light source against a white backdrop, yielding high contrast and clarity at elevated frame rates. Each experimental run lasted 0.93 s, capturing the inception, growth, and breakup of interfacial waves with sufficient temporal and spatial resolution for quantitative image analysis.

 doi:10.20944/preprints202605.0783.v1



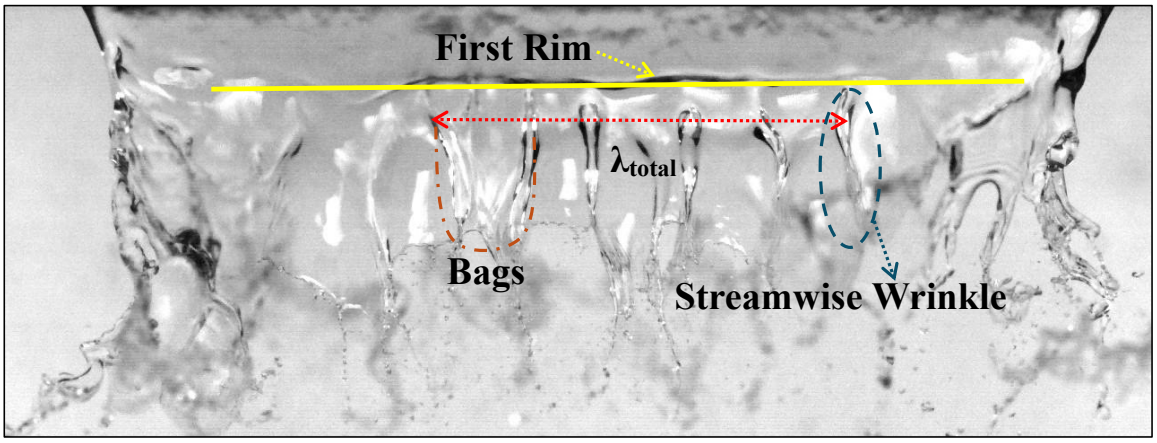


**Figure 2.** Definition of transversal wavelength where $\lambda_{tra} = \lambda_{total}/\mathrm{n}$ where n is the number of waves intercepted.

### *1.2. Preliminary Results*

The parameter $M = \dfrac{(\rho_g V_g^2)}{(\rho_\ell V_\ell^2)}$ is used here as a measure of aerodynamic forcing: it compares the gas dynamic pressure to the liquid dynamic pressure and therefore quantifies the ability of the gas flow to accelerate and deform the film relative to the film's inertia. $M$ is widely used in air-blast atomization studies because it compactly links gas momentum flux to liquid feed conditions and often correlates with the transition between breakup modes (e.g., rim/ligament versus hole/bag breakup). Figure 3 (a1 & a2) and (b1 & b2) illustrate that, even when the dynamic pressure ratio is fixed, the transverse wavelength $\lambda_{\mathrm{tra}}$ varies significantly with $M$. Wavelengths were measured by drawing a red line across multiple ligaments and dividing their length by the number of full waves intercepted. For $M = 6$, cases (a1) and (a2) yield $\lambda_{\mathrm{tra}} = 2.30\,\mathrm{mm}$ at $(V_g, V_l) = (54, 0.77)\,\mathrm{m/s}$ and $\lambda_{\mathrm{tra}} = 6.46\,\mathrm{mm}$ at $(V_g, V_l) = (22, 0.32)\,\mathrm{m/s}$. Similarly, at $M = 8$, subfigures (b1) and (b2) give $\lambda_{\mathrm{tra}} = 1.91\,\mathrm{mm}$ for $(V_g, V_l) = (61, 0.77)\,\mathrm{m/s}$ and $\lambda_{\mathrm{tra}} = 3.00\,\mathrm{mm}$ for $(V_g, V_l) = (44, 0.55)\,\mathrm{m/s}$. These results demonstrate that a similar dynamic pressure ratio $M$ does not fix the interfacial wavelength; both absolute gas and liquid speeds influence the instability scale. Note that the density ratio $\rho_g/\rho_\ell$ was kept constant while changing the dynamic pressure ratio. The vertical error bars on $\lambda_{\mathrm{tra}}$ indicate the cumulative uncertainty of $\pm 4.01\%$, obtained by combining instrument calibration, imaging resolution, and post-processing uncertainties. These bars are plotted for each data point to convey the measurement confidence.

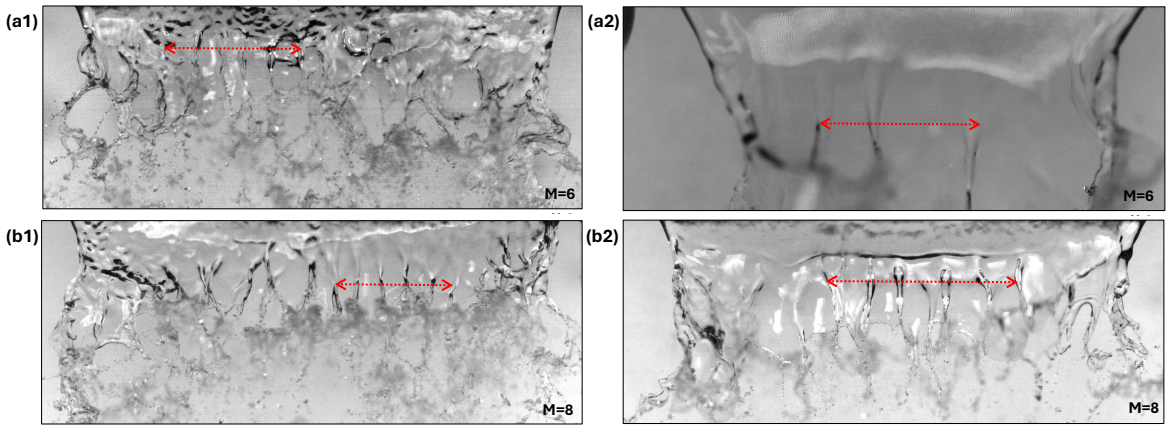


**Figure 3.** Transverse wavelength measurement for fixed dynamic pressure ratio $M = (\rho_g V_g^2)/(\rho_\ell V_\ell^2)$. In each subfigure, the red horizontal line spans several ligaments; $\lambda_{\mathrm{tra}}$ is obtained by dividing its length by the number of wavelengths intercepted. (a1) $M = 6$, $V_g = 54\,\mathrm{m/s}$, $V_\ell = 0.77\,\mathrm{m/s}$, $\lambda_{\mathrm{tra}} = 2.30\,\mathrm{mm}$. (a2) $M = 6$, $V_g = 22\,\mathrm{m/s}$, $V_\ell = 0.32\,\mathrm{m/s}$, $\lambda_{\mathrm{tra}} = 6.46\,\mathrm{mm}$. (b1) $M = 8$, $V_g = 61\,\mathrm{m/s}$, $V_\ell = 0.77\,\mathrm{m/s}$, $\lambda_{\mathrm{tra}} = 1.91\,\mathrm{mm}$. (b2) $M = 8$, $V_g = 44\,\mathrm{m/s}$, $V_\ell = 0.55\,\mathrm{m/s}$, $\lambda_{\mathrm{tra}} = 3.00\,\mathrm{mm}$.

 doi:10.20944/preprints202605.0783.v1



Figure 4 shows that increasing the gas velocity from $V_g = 22\,\mathrm{m/s}$ to $64\,\mathrm{m/s}$, more than doubling, causes the transverse wavelength $\lambda_{\mathrm{tra}}$ to decrease dramatically from about 6.5 mm to 1.6 mm approximately at a fixed $V_\ell = 0.32$. By contrast, changing the liquid-phase velocity across $V_\ell = 0.32$–$0.77\,\mathrm{m/s}$ produces only minor variations in $\lambda_{\mathrm{tra}}$ at each fixed $V_g$. Hence, the instability wavelength is governed primarily by the gas-shear intensity, with the liquid inflow rate playing only a secondary role under our conditions.

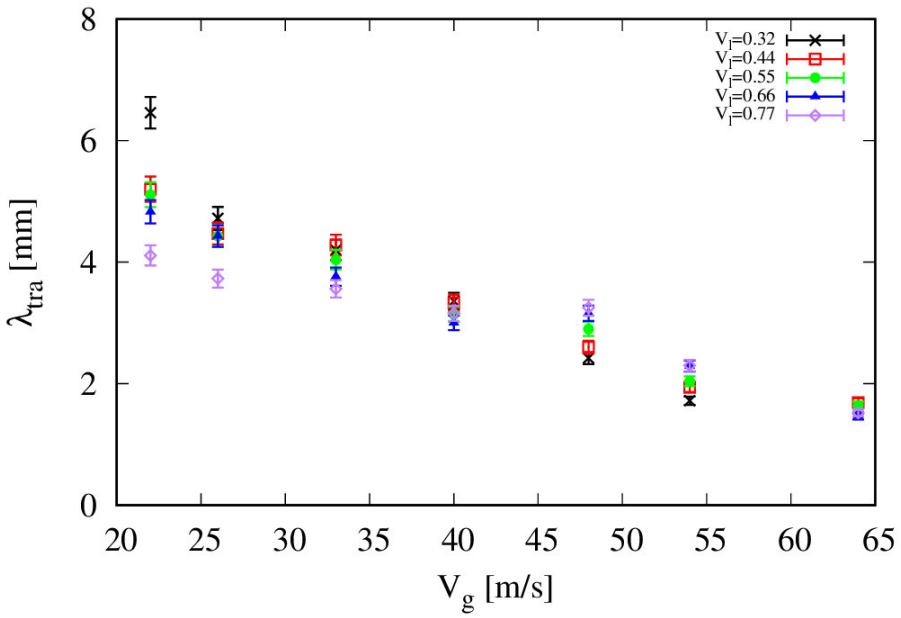


**Figure 4.** Variation of transverse wavelength $\lambda_{\mathrm{tra}}$ with gas velocity $V_g$ for five liquid-phase velocities $V_\ell$. Symbols: $\times$ ($V_\ell = 0.32\,\mathrm{m/s}$), $\square$ ($0.44\,\mathrm{m/s}$), $\circ$ ($0.55\,\mathrm{m/s}$), $\triangle$ ($0.66\,\mathrm{m/s}$), $\diamond$ ($0.77\,\mathrm{m/s}$).

## 2. Conclusions

We have experimentally investigated the initial instability and primary breakup of a planar liquid film sheared by symmetric, high-speed gas streams. High-speed imaging of a $D_\ell \approx 150\ \mu$m film revealed that the transverse wavelength $\lambda_{\mathrm{tra}}$ is strongly controlled by the gas-side shear: increasing $V_g$ from 22 to $64\,\mathrm{m/s}$ reduces $\lambda_{\mathrm{tra}}$ from 6.5 mm to 1.6 mm. By contrast, changes in the liquid inflow $V_\ell$ across 0.32–$0.77\,\mathrm{m/s}$ produce only modest shifts in $\lambda_{\mathrm{tra}}$ at fixed $V_g$. Crucially, a fixed dynamic pressure ratio $M = (\rho_g V_g^2)/(\rho_\ell V_\ell^2)$ does not uniquely determine the instability scale: different $(V_g, V_\ell)$ pairs with the same $M$ yield distinct wavelengths.

These findings imply that gas-side flow structures set the dominant length scales for primary breakup, with the liquid flux modulating but not dictating the instability wavelength under the tested conditions.

**Data Availability Statement:** The data that support the findings of this study are available from the corresponding author upon reasonable request.

## References

1. Esfarjani, S.A.; Dolatabadi, A. A 3D simulation of two-phase flow in an effervescent atomizer for suspension plasma spray. *Surface and Coatings Technology* **2009**, *203*, 2074–2080.
2. Qian, L.; Lin, J.; Xiong, H. Modeling of non-Newtonian suspension plasma spraying in an inductively coupled plasma torch. *International journal of thermal sciences* **2011**, *50*, 1417–1427.
3. Jerome, J.J.S.; Marty, S.; Matas, J.P.; Zaleski, S.; Hoepffner, J. Vortices catapult droplets in atomization. *Physics of Fluids* **2013**, *25*, 112109.
4. Oshima, I.; Sou, A. Longitudinal oscillation of a liquid sheet by parallel air flows. *International Journal of Multiphase Flow* **2019**, *110*, 179–188.

 doi:10.20944/preprints202605.0783.v1



5. Chandra, N.K.; Sharma, S.; Basu, S.; Kumar, A. Aerodynamic bag breakup of a polymeric droplet. *arXiv preprint arXiv:2309.14729* **2023**.
6. Jackiw, I.M.; Ashgriz, N. Prediction of the droplet size distribution in aerodynamic droplet breakup. *J. Fluid Mech.* **2024**, *940*.
7. Oshima, I.; Sou, A. Air-blast atomization of a liquid film. *Journal of Fluid Mechanics* **2024**, *985*, A36.
8. Agbaglah, G.G. Numerical study of hole formation in a thin flapping liquid sheet sheared by a fast gas stream. *Physics of Fluids* **2021**, *33*.
9. Fernández, V.G.; Berthoumie, P.; Lavergne, G. Liquid sheet disintegration at high pressure: An experimental approach. *Comptes Rendus Mécanique* **2009**, *337*, 481–491.
10. Osama, M.; Agbaglah, G.G. From vortices to droplets: Gas-phase instability effects on thin liquid film breakup. *Physics of Fluids* **2025**, *37*.